Eye-safe aerosol lidar at 1.5 microns: progress towards a scanning lidar network

Scott M. Spuler and Shane D. Mayor

National Center for Atmospheric Research, P.O. Box 3000, Boulder CO, USA

ABSTRACT

A multi-dimensional scanning lidar has been developed for tracking and monitoring aerosol plumes in urban settings. The reliability of the system has been demonstrated and plans for additional units are in place to create a unique scanning lidar network. The paper discusses the current capabilities of the instrument and research underway to extract more information, such as quantitative aerosol properties, from the network.

Keywords: eye-safe lidar, aerosol, environmental monitoring

1. INTRODUCTION

Three-dimensional measurements of the lower atmospheric boundary layer in urban areas can provide information on aerosol distribution properties where much of our population live and work. Although many different types of lidar systems exist, only a select subset are well-suited for aerosol research – and of this group, most have limitations associated with range, resolution, and/or eye-safety for this type of measurement. For example, although traditional micropulse lidars[1] are inexpensive, eye-safe, and reliable, they do not provide high temporal resolution and long-range data simultaneously and are therefore not suited for scanning. A scanning lidar is necessary to enable important multi-dimensional views of the atmosphere and acquire spatial information which is impossible to achieve with other ground-based vertically pointing lidars (see Fig. 1 and Fig. 2). For example, vertical scanning enables collection of data all the way down to surface of the earth itself, while horizontal scanning can reveal the location of point sources of particulate matter and the location and size of aerosol plumes. The ideal lidar, optimized for scanning from the ground, should (1) transmit high pulse-energy to enable rapid scanning in multiple dimensions; and (2) be eye-safe to permit continuous and unattended operation in urban areas.

Over the past several years the National Center for Atmospheric Research (NCAR) has been developing an elastic backscatter lidar called the Raman-shifted Eye-safe Aerosol Lidar (REAL).[2–4] The system is presently field deployable through NCAR and provides animations of atmospheric structure as revealed by variability in the aerosol optical scattering in horizontal and vertical planes. The top requirement for the instrument was eye-safety with high pulse energy for long-range and rapid-scanning – so the wavelength was selected to be within the safest wavelength region (1.5 - 1.8 μm) in the entire optical spectrum (see Fig. 3). Furthermore, molecular backscattering from laser radiation in this wavelength region is relatively weak compared to aerosol backscattering. Therefore, the large dynamic range of a lidar return signal at this wavelength region results mainly from the one-over-range-squared dependence of aerosol scattering – resulting in excellent sensitivity to small changes in aerosol backscatter cross-section.

In addition to the field-transportable NCAR-REAL, a permanent version was created in 2005 for continuous and unattended surveillance of aerosol plumes in Washington DC (see Fig. 4). Two additional REALs are currently being procured for the National Capital Region and for Dugway Proving Ground, Utah. This work is being accomplished by a contractor with a tech-transfer licensing agreement with NCAR. Because these instruments are designed to run continuously and unattended, the data they produce could potentially provide long-term trends of the spatial distribution of aerosol optical information in urban environments. NCAR staff work closely with the contractor producing the REAL technology to ensure a mutually beneficial flow of design and performance information. We expect that this tech-transfer activity will result in increasingly reliable, lower-cost, and higher performance instruments.

Further author information: (Send correspondence to S. Spuler)
E-mail: spuler@ucar.edu, Telephone: 303 497 2014

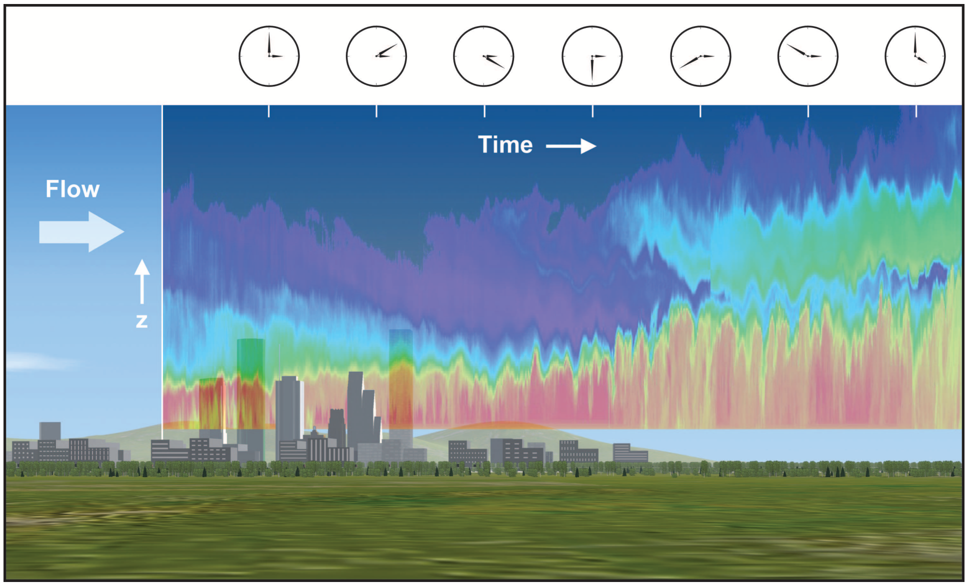

Figure 1. Ground-based zenith-pointing lidars are limited to providing time history versus altitude data.

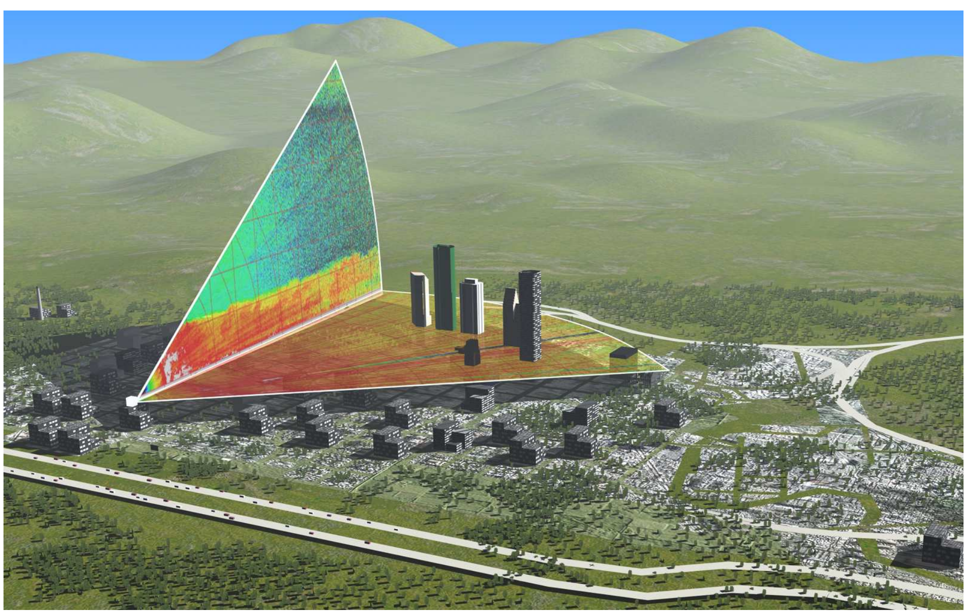

Figure 2. Ground-based scanning lidars can provide data on both horizontal and vertical planes. The two different scans can be interleaved sequentially in order to provide both horizontal and vertical animations over the same time period.

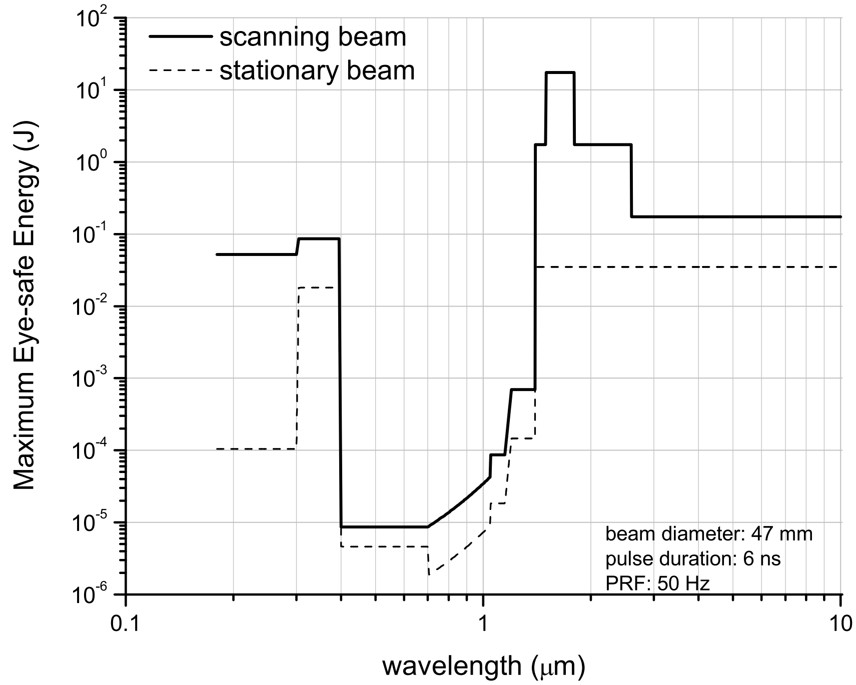

Figure 3. Maximum eye-safe energy vs. wavelength based on the American National Standard for Safe Use of Lasers, ANSI Z136.1-2000, for the conditions shown. The solid line is calculated for a single pulse exposure. The dashed line is calculated for multiple pulses, or stationary laser beam conditions, with exposure times based on the natural aversion time of the human eye – 0.25 second and 10 seconds for inside and outside the visible wavelength region; respectively. This figure was copied from Spuler and Mayor, 2007.[4]

Figure 4. The first REAL "v2" created through a tech-transfer licensing agreement between a commercial firm and NCAR. The unit operates continuously (except for flashlamp changes every 2 weeks) and unattended for the automatic detection and tracking of aerosol plumes in Washington DC.

This paper provides an overview of the current capabilities of the instrument (e.g., atmospheric flow visualization), its impact for a broader reach via urban networks, and details of some of our ongoing and future work to improve instrument performance such as the ability to classify plume types via depolarization and quantitative measurement of aerosol properties.

2. CURRENT CAPABILITIES

The Raman-shifted Eye-safe Aerosol Lidar was created to provide the community with a field-deployable, eye-safe, scanning lidar for weather and climate research. In its present configuration REAL can routinely observe atmospheric structure to ranges of 5 to 10 km during clear weather conditions. It can operate unattended for periods of approximately 28 days. At this point, the laser flash lamps must be replaced which is a straightforward procedure that requires less than 30 minutes. Raw data, stored on high capacity external hard disks, are also replaced during visits to change flashlamps. "Quicklook" images of the scan data are uploaded to NCAR via an internet connection approximately once per minute. These images are stored on a server where they can be accessed and animated by anyone with a web-browser and internet service. All features of REAL operation are controlled by a Labview program running under Windows XP which can be accessed remotely via an internet connection. Lidar scan strategies can be changed and system performance can be monitored. The beam steering unit can be programmed to collect any combination of elevation (vertical) and azimuthal (horizontal) scans.

The field-deployable NCAR-REAL has participated in six field experiments since 2004. These have occurred in diverse locations such as Washington DC, Albuquerque NM, Dugway UT, Independence CA, Dixon CA, and its home-base of Boulder, CO. The large power-aperture product of REAL results in excellent performance in atmospheres with a wide range of backscatter and extinction conditions. We have collected thousands of hours of data on boundary layers, clouds, and various types of particulate plumes. Currently, the data are primarily used to elucidate atmospheric structure and dynamics in mesoscale and microscale meteorological studies.

An example of a vertical scan from the most recent deployment of REAL is shown in Figure 5. Note that the optical scattering in a convective boundary layer can be quite inhomogeneous. Mixing and sources of pollutants can cause tremendous changes in optical scattering over relatively short distances. Within the ABL in this figure, the backscatter intensity changes from 33 dB to over 40 dB in as little as 100 meters horizontal and vertical distance. The lidar is also sensitive to optically-thin aerosol layers above the atmospheric boundary layer. In the figure, several layers from 1.0 to 3.3 km elevation are evident. The full-hemispheric scanning allows the lidar to probe all the way down the bottom of the atmosphere. The instrument is capable of providing very high vertical resolution (approximately 1 meter at 1-km range) data all the way down to the tree tops if it is given an appropriate vantage. Fig. 6 is a single horizontal sector scan from REAL's first deployment in Washington DC in May of 2004.[5] The location of the lidar was such that it was possible to scan at a zero-degree elevation angle to a range of azimuth angles to the east. This scan plane is collected just 10's of meters above the heart of Washington, D.C. This *sector scan* took approximately 20 s to acquire. Here we also see backscatter intensity changes of at least 8 dB over horizontal distances of less than 100 meters. Animations of this data reveal many sources and complex dispersion paths.

2.1 Instrument Reliability

REAL uses a Raman shifter – stimulated Raman scattering in methane – to convert 1-micron pump radiation to 1.5-microns wavelength. Historically this type of cell has required frequent optics cleaning, provided poor beam quality and has limited pulse repetition frequency (PRF). As a result of these problems, the technique earned a reputation for poor reliability and was understandably dismissed by many searching for a lidar transmitter at this wavelength.[6] However, as discussed in Spuler and Mayor[4] , it is possible to overcome these problems and the Raman shifter used in the REAL system has continued to prove reliable. As an example of this documented reliability, Figure 7 shows the transmitter performance for the most recent deployment of REAL in Dixon CA from 13-March to 13-June 2007. The system was continuously operated (24/7) for the nearly 90 day project except for 3 brief periods. Two episodes were due to electrical brown-outs and required only a reset (the first tripped the AC unit and the second tripped the laser power supply) the third outage was required to a replace a failed commercial off-the-shelf data acquisition board. The sawtooth appearance of output power in the lower trace of Fig. 7 is due to voltage corrections applied to the pump laser flashlamps over their lifetime. Prior to

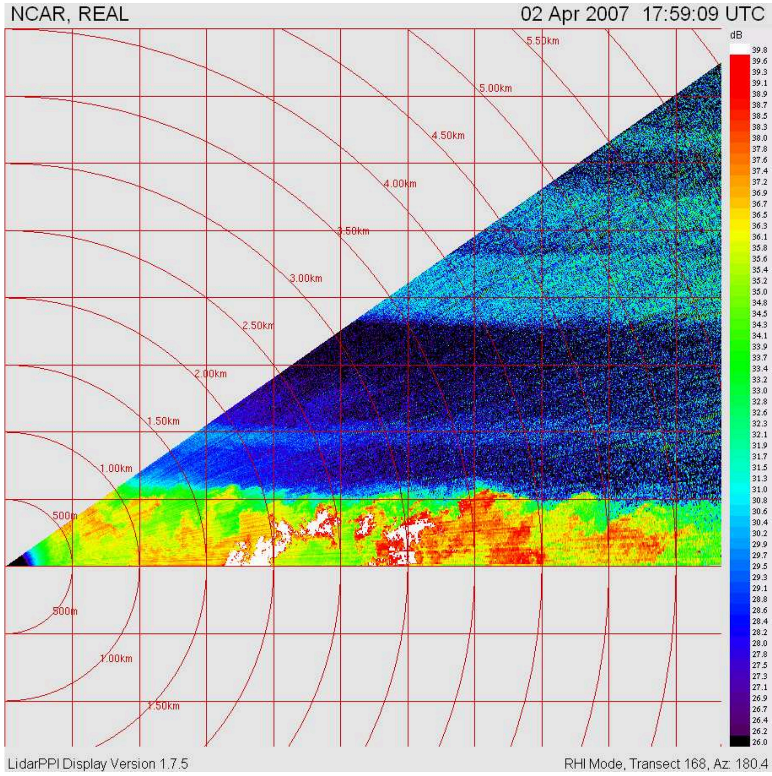

Figure 5. Vertical scan from the NCAR REAL in Dixon, California, showing a clear, convective, atmospheric boundary layer.

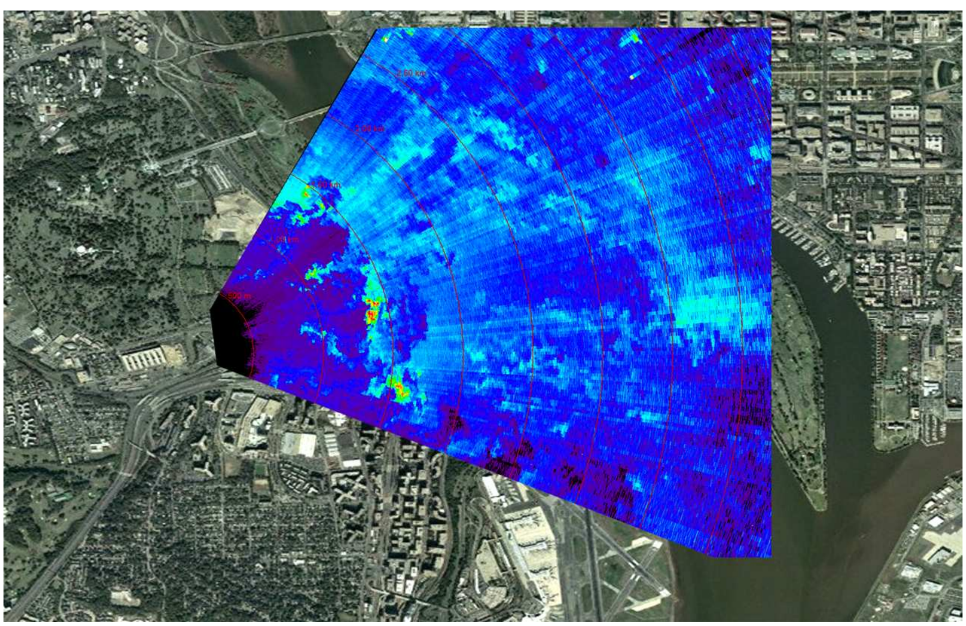

Figure 6. Horizontal scan from the NCAR REAL in Washington, D.C., on 7 May 2004 superimposed on an aerial photograph showing microscale variability of relative optical scattering.

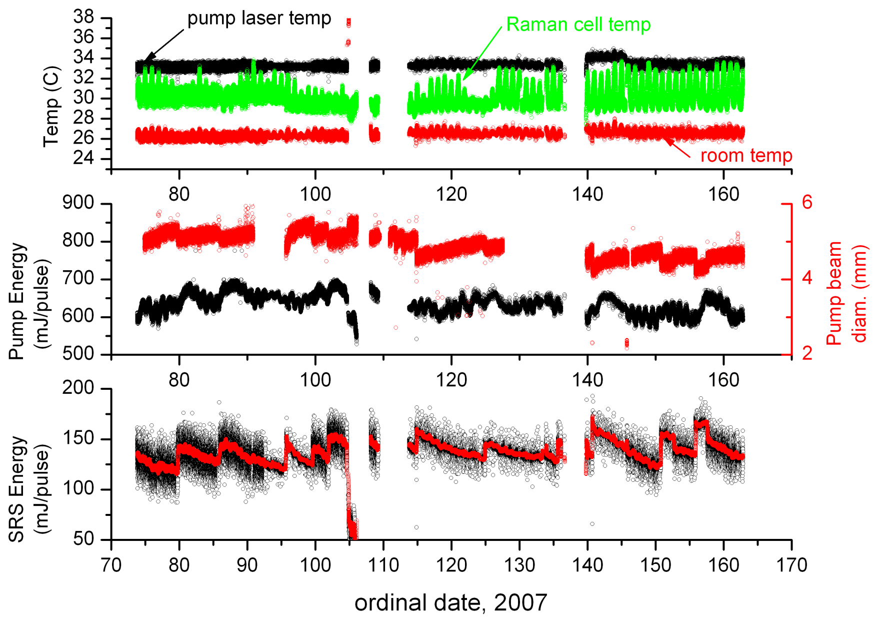

Figure 7. System performance parameters from the most recent deployment of REAL. The output laser energy (SRS energy plot) shows no sign of degradation of performance throughout the 90 day project. The blank periods were due to two electical brown outs in the middle of the project and a replacement of the data acquisition board at ordinal date 137.

the field project, the system endured a stability test which ran from 16-October to 1-December, 2006. For the first 2 weeks of this test the system was running only during the weekdays –afterwards it was operational 24/7 – for about 38 days equivalent continuous operation. During the combined period of initial tests and the field project, the Raman cell required zero maintenance and there was no performance degradation during its ∼2,800 hours of operation.

2.2 Aerosol Depolarization Measurements

Backscatter polarization sensitivity was added to the NCAR-REAL in 2005. This was accomplished by improving the linear polarization purity of the transmitter and adding a polarization beam-splitter and second channel to the receiver. The system was taken to Dugway Proving Ground for testing with various forms of particulate matter (i.e. droplets and crystals). Results show that the lidar is sensitive to the relative depolarization ratio which can be used as a marker for plume identification. Figure 8 shows an example of data collected where two aerosol plumes were deliberately created at different locations. One is composed of droplets and the other is composed of dry, non-spherical, particles. The data show that these microphysical properties are reflected in the lidar data. These results are summarized in a paper scheduled to appear in the September 2007 of *Optical Engineering*.[7] We note that although many papers discuss polarization lidar for cloud research,[8] few polarization observations of lower tropospheric aerosols exist.

For more accurate depolarization measurements, the mirrors through which the laser beam is re-directed, or scanned, (as well as collect backscatter from the atmosphere) must be specially coated to eliminate systematic polarization errors. The present scanning mirrors are coated with protected gold which, as discussed in Mayor *et al.*,[7] have a well matched reflectivity between the S and P polarization states; however, induce phase shifts as a function of scan angle. These phase shifts result in systematic errors when measuring the depolarization ratio. We are currently working to replace these mirrors with a set coated with a dielectric stack designed to minimize the phase shift at the transmitted wavelength. This will allow robust measurement of the depolarization ratio regardless of the BSU scan angle.

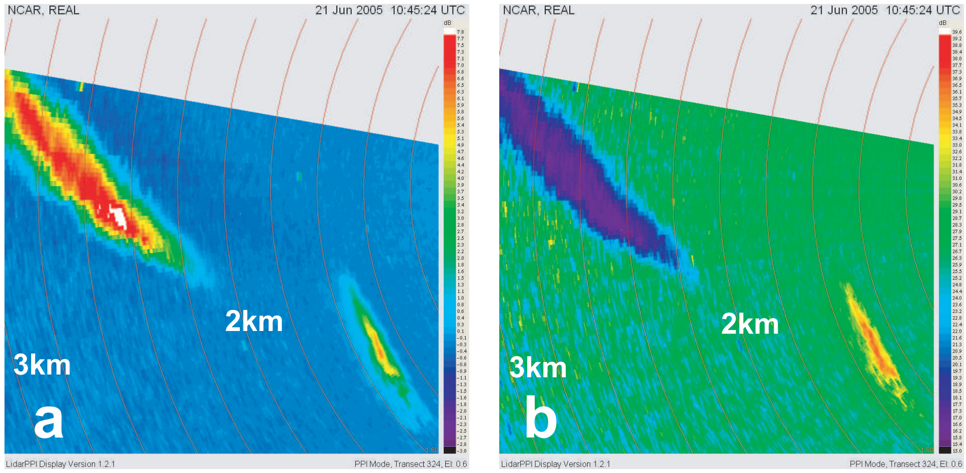

Figure 8. A single horizontal scan through two different types of aerosol plumes at Dugway Proving Ground. Left panel (a): total backscatter intensity. Right panel (b): backscatter depolarization ratio. The low depol-ratio plume was composed of droplets while the high-depol ratio plume was composed of non-spherical particles (road dust). These results will appear in Mayor et al. 2007.[7]

3. CURRENT RESEARCH

The data examples heretofore mentioned are capable of showing the relative changes of optical scattering, and thus atmospheric structure and motion. Note that in both Figs. 5 and 6 the data are in uncalibrated physical units of digitizer counts displayed in decibels (dB). Therefore, the absolute magnitude of the data will change if hardware changes, such as electronic gain settings, digitizer settings, or changes in the reflectivity or transparency of mirrors and windows occur.

With a prototype scanning lidar network based on this lidar technology being considered in the National Capitol Region, it would be advantageous to assign physical units to the data so comparisons can be drawn from observations made at different times and locations and from different instruments. One possibility is to use calibration techniques that include using targets (wires or boards with known reflectivity) or aerosol free regions of the atmosphere. Unfortunately, these methods employ assumptions that contain potentially large errors. A more robust calibration – using the natural molecular signal at each point in range as a reference signal – can be accomplished using the high spectral resolution lidar (HSRL) technique. This technique would be more difficult to implement but has the potential to provide more accurate data. The first HRSL works appear to be published in 1983 by two groups: Colorado State University[9] and the University of Wisconsin.[10,11] The basic concept of technique can best be understood starting with the lidar equation, describing the backscattered optical power (P) as a function of range (R):

$$P(R) = E\frac{c}{2}\eta\frac{A_r}{R^2}O(R)\left[\beta_a(R) + \beta_m(R)\right]\ \exp\left[-2\int_0^{\mathrm{R}}(\alpha_{\mathrm{a}}(\mathrm{R}') + \alpha_{\mathrm{m}}(\mathrm{R}'))\mathrm{dR}'\right] \tag{1}$$

where E is the pulse energy of the laser, c is the speed of light, A_r is the area of the receiver, η is the receiver efficiency, O is the laser-beam receiver field-of-view overlap function, β is the backscatter coefficient for aerosols and molecules (subscript a and m; respectively), and α is the extinction for aerosols and molecules (subscript a and m; respectively).

The four atmospheric unknowns (β_a, β_m, α_a, and α_m) cannot be solved for with this single equation. Therefore, the HSRL technique strives to separates the molecular return from the aerosol return (discussed later) into two simultaneous measurements. The returned optical power from molecules can be well estimated from Rayleigh theory – the small size of the air molecules with respect to the wavelength of the transmitted light place these scattering properties (backscatter and extinction) in a well defined regime. For example, the molecular backscatter cross section for air is given by:

$$\sigma_m(R) = \left[\frac{\pi^2(n_{air}^2-1)^2}{N(R)^2\lambda^4}\right] \quad \text{or} \quad 5.45\left(\frac{550\ \text{nm}}{\lambda}\right)^4\ 10^{-28}\ \text{cm}^2\ \text{sr}^{-1} \tag{2}$$

where λ is the wavelength of the light transmitted, and n_{air} is the index of refraction for air, and the molecular number density $N(R)$ is given as:

$$N(R) = \frac{P_{air}(R)}{T_{air}(R)k_B} \tag{3}$$

where P_{air} is the air pressure, T_{air} is the air temperature, and k_B is the Boltzmann constant. The molecular backscatter and extinction terms can then be written as

$$\beta_m(R) = N(R)\sigma_m(R) \quad \text{and} \quad \mathrm{\alpha_m(R) = \frac{8\pi}{3}N(R)\sigma_m(R)} \tag{4}$$

In this manner the equation is separated into two simultaneous measurements results in two equations with only two unknowns (the aerosol scattering terms β_a, α_a) which can be solved. In this way, measurements from each in the lidar return are referenced to a simultaneous molecular scattering measurement at that point.

The separation of the signals exploits the fact that the molecular and aerosol backscatter have different spectral widths. The molecular return is broadened by its large velocity distribution compared to aerosols due to their difference in mass. The velocity distribution can be given by the Maxwell-Boltzmann distribution in a single direction

$$f(v) = \sqrt{\frac{M_{air}}{2\pi k_B T_{air}}}exp\left(\frac{-M_{air}v^2}{2k_B T_{air}}\right) \tag{5}$$

where, v is the velocity, M_{air} is the molecular weight of air (28.95 amu), and k_B is the Boltzmann constant, and T_{air} is the air temperature. Note that the air temperature and pressure must be estimated for the HSRL technique. It follows that this velocity distribution results in a backscattered Doppler shift which can be given by

$$f_D(v) = 2v/\lambda \tag{6}$$

where v is the velocity and λ is the wavelength of the transmitted light.

As seen from the above equations, implementing the HSRL technique at REAL's relatively long wavelength is challenging. First, the spectral width of the molecular return is approximately 3 times narrower than if operating in the 532-nm region. At an air temperature of 290K the expected Doppler width is ∼880 MHz full width at half maximum (FWHM). Second, as seen in Eq. 2 the molecular cross section – scaling as the inverse wavelength to the fourth power – will be two orders of magnitude less than if operating at 532-nm. At standard temperature and pressure, the molecular backscatter coefficient will be 2×10^{-8} m^{-1} sr^{-1}.

The first steps to demonstrate that the REAL transmitter is capable of the necessary spectral purity for HSRL are published in a May 2007 *Applied Optics* paper.[4] In summary, the linewidth of the transmitter was narrowed by using two different injection seed lasers. A fiber laser injection seed was used on the Nd:YAG pump laser and a telecom diode laser was used as a seed for stimulated Raman scattering in the wavelength converter. The new transmitter was also shown to be capable of almost twice the pulse energy and 5 times higher pulse repetition rate than our current fieldable REAL. With this, we demonstrated over 17 W where the fieldable REAL transmits less than 2 W. The transmitted laser linewidth was shown to be approximately 175 MHz (1.6 pm) and capable of a small tuning range necessary for HSRL.

To separate the molecular backscatter return from the aerosol return, two separate optical paths or channels are used in the receiver. In one channel, the combined return is simply focused onto a photodetector; however, in the other channel a narrow spectral filter is used to block the aerosol signal from reaching the photodetector.

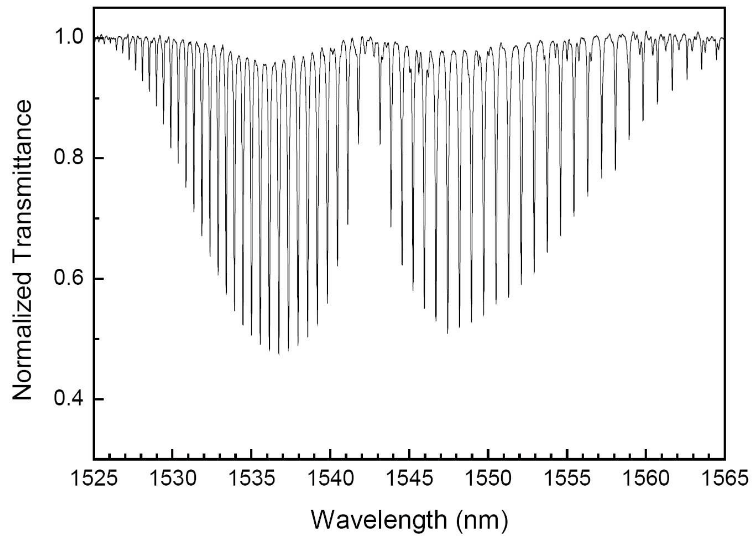

Figure 9. Transmission spectrum of $H^{13}CN$.

HSRL systems at 532-nm have been successful employing atomic gas (iodine) filters for this purpose. However, in the near IR, there are no atomic gas ground state transitions so we looked to create the filter from a molecular gas – generally with much weaker line strengths.

In the telecommunications c-band, which spans the wavelength region in which REAL operates, HCN absorption lines are used as a standard wavelength reference.[12] The absorption spectrum of this gas is shown in Fig. 9. As a first check if HCN could be a suitable filter gas – or sufficiently narrower than the Doppler width of the air molecular return – one can look at its mass. The mass of HCN and air (28.95 amu) are roughly the same, therefore the HCN filter width should approach roughly half the width of the air backscatter return in the absence of collisional broadening (i.e., at low pressure). This is because the Doppler width is doubled when the light is backscattered (note Eq. 6). Therefore, to keep the filter width sufficiently narrow, low pressures – on the order of 1 Torr – must be used. The necessary low pressure, coupled with the weakly absorbing molecule requires a long interaction length between the light and the gas to obtain sufficient absorption.

We have demonstrated that two of the HCN rotational-vibration transitions (the P_2 line of $H^{13}CN$ and the P_{13} line of $H^{12}CN$) are within the tuning range of our next generation transmitter.[4] The P(13) line of $H^{12}CN$ was the stronger of the two transitions and also is free from interfering hot bands. Therefore for a demonstration of the technique, we developed an absorption filter from this line at pressure of 1 Torr in a 1.5 meter folded path length cell design. This path length was chosen since it is the maximum path at which receiver efficiency as a function of range (i.e, overlap function) is not adversely affected with the current optical configuration. Figure 10 shows the gas filter performance – including the transmission of the air molecular return and aerosol return. When the laser wavelength is at the filter center, 54% of the molecular backscatter return is transmitted through the filter while 36% of the aerosol return is transmitted through the filter. These transmission coefficients must be accounted for when solving the backscatter and extinction terms. The cross-talk between channels, due to the transmission of aerosol signal in the filtered channel, limits the measurement of backscatter coefficients to those less than approximately 10^{-7} m^{-1} sr^{-1}. In other words, the measured channel ratio (filtered channel/combined channel) will be the same for all backscatter coefficients greater than 10^{-7} m^{-1} sr^{-1}. While the cross-talk between channels defines the upper limit, the noise floor limits the ability to measure weaker backscatter coefficients. For a 1 minute average (250 mJ, 25 Hz PRF system) the weakest measurable backscatter coefficient is estimated to be around 5×10^{-9} m^{-1} sr^{-1}. Therefore, the instrument, using the free space 1.5 path gas cell, has limited range of aerosol backscatter levels that are quantifiable or that can be used as a means of calibration.

This type of filter could; however, provide a calibration comparable to that of a known hard target under certain conditions. This would have the advantage of not requiring space for the targets and all the associated uncertainties such as (1) two-way extinction, (2) target reflectivity (3) bandwidth response issues, etc.. For

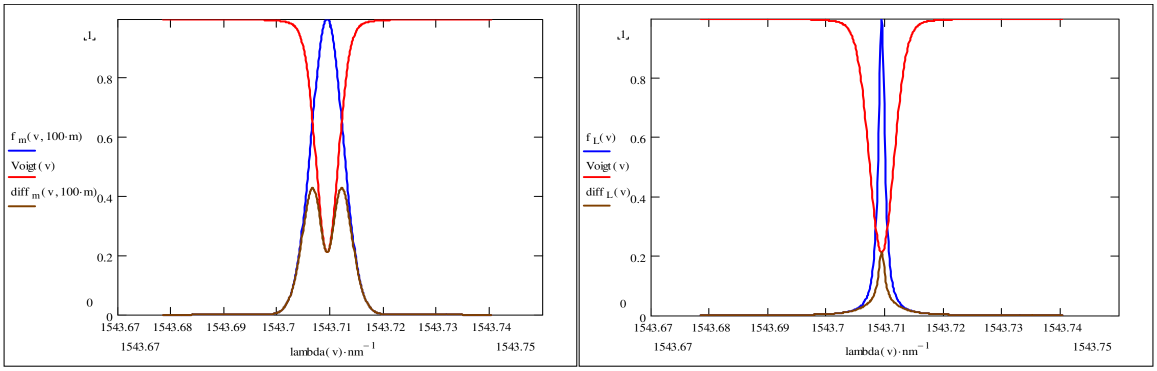

Figure 10. Left: Filter performance for passing the molecular return. Blue: dry air molecular backscattering resulting from narrow laser before filter. Red: filter transmission from the P13 line of HCN (1 Torr, 1.5 meter path length). Brown: molecular backscattering transmission after filter. Right: Filter performance for blocking the aerosol return. Blue: aerosol/laser backscatter before filter. Red: filter transmission from the P13 line of HCN (1 Torr, 1.5 meter path length). Brown: aerosol backscatter transmission after pass through filter.

example, with the present cell a potential calibration procedure could be performed where the system was pointed vertically for 1 minute during stable atmospheric conditions with shallow boundary layer without cloud cover. The transition from the boundary layer to the relatively clean air above would act as a target to calibrate the system as long as this region of air had the required backscatter coefficient range of 5×10^{-9} m^{-1} sr^{-1} to 10^{-7} m^{-1} sr^{-1}. Increased absorption by means of a longer interaction path length or using a different filter type – such as an etalon – will be required to expand the measurement capability to a larger range of backscatter coefficients and improve performance. One potential means to a longer path-length is discussed below.

4. FUTURE WORK

We plan to investigate using a photonic crystal fiber (PCF) filled with low-pressure HCN to replace our current multi-pass cell. The fiber may provide a longer path and therefore greater suppression of the aerosol signal. If successful, it will also eliminate depth-of-field challenges associated with increasing path length beyond 1.5 meters using free-space optics, and provide a more compact and alignment-insensitive absorption filter. We plan to investigate employing an air-clad, multi-mode photonic crystal fiber for this purpose. The outer ring of holes in such a fiber separate the core from the cladding and are used in increase the numerical aperture (NA) of the fiber and allow for a steep entrance light cone. Ideally, these holes can be filled with HCN in a manner similar to that described in Tuominen *et al.*[13] however, a long length fiber must be used to offset the reduced efficiency of the evanescent wave interaction with the gas (i.e., the light will travel mostly through the solid silica core). Some air-clad PCFs also contain holes within the core which are designed to guide a single-mode in the center. We plan to also investigate use of such a fiber design for the additional interaction with the filter gas they will provide. Air-clad PCFs with 200 μm diameter cores fibers are commercially available with lengths up to 50-m. The relatively large diameter and high NA of these fibers will allow the custom focusing optics used in the present receiver configuration to be retained.

5. CONCLUSIONS

National security, short-term weather forecasting, climate studies, and air-quality monitoring would all benefit from networks of scanning aerosol lidars – particularly if calibrated. A multi-dimensional scanning lidar well suited for urban surveillance and aerosol plume monitoring has been developed and is operational. Details of the current instrument capabilities are given including (1) its ability to provide detailed time-lapse animations of relative aerosol backscatter in horizontal and vertical planes (2) frequency converter reliability results and (3) aerosol depolarization measurement capability.

Research is underway to assign physical meaningful units to the data so comparisons can be drawn from observations made at different times and locations and from different instruments. For this purpose, use of the high spectral resolution lidar technique is currently under investigation – using the natural molecular reference signal as a means of calibration. To date, investigation into molecular gas absorption cells to provide a suitable notch filter for the technique has provided limited success. Longer absorption paths or etalon based filters will be necessary to more accurately measure a wider range of aerosol backscatter coefficients.

ACKNOWLEDGMENTS

The authors would like to thank Dr. Edwin Eloranta for helpful discussions and Mr. Bruce Morley for design and operation of the data acquisition and lidar control system. The work builds upon investments by the National Science Foundation (NSF) and the National Center for Atmospheric Research (NCAR) since 2001.

REFERENCES

1. J. D. Spinhirne, "Micropulse lidar," *EEE Trans. Geoscience and Remote Sensing* **31**, pp. 48–55, 1993.
2. S. D. Mayor and S. M. Spuler, "Raman-shifted eye-safe aerosol lidar," *Appl. Optics* **43**, pp. 3915–3924, 2004.
3. S. M. Spuler and S. Mayor, "Scanning eye-safe elastic backscatter lidar at 1.54 microns," *J. Atmos. Ocean. Technol.* **22**, pp. 696–703, 2005.
4. S. M. Spuler and S. D. Mayor, "Raman shifter optimized for lidar at 1.5-micron wavelength," *Appl. Optics* **46**, pp. 2990–2995, 2004.
5. T. Warner, P. Benda, S. Swerdlin, J. Knievel, E. Argenta, B. Aronian, B. Balsley, J. Bowers, R. Carter, P. A. Clark, K. Clawson, J. Copeland, A. Crook, R. Frehlich, M. L. Jensen, Y. Liu, S. Mayor, Y. Meillier, B. Morley, R. Sharman, S. Spuler, D. Storwold, J. Sun, J. Weil, M. Xu, A. Yates, and Y. Zhang, "The pentagon shield program toward critical infrastructure protection," *Bull. Amer. Meteor. Soc.* **88**, pp. 167–176, 2007.
6. V. A. Kovalev and W. E. Eichinger, *Elastic lidar*, John Wiley and Sons, New Jersey, 2004.
7. S. M. S. Mayor, S. D., B. M. Morley, and E. Loew, "Polarization lidar at 1.54-microns and observations of plumes from aerosol generators," *Optical Engineering* **in press for September issue**, 2007.
8. K. Sassen, *Lidar backscatter depolarization technique for cloud and aerosol research*, ch. Chapter 14 of Light scattering by non-spherical particles, pp. 393–673. Academic Press, 2000.
9. H. Shimizu, S. A. Lee, and C. Y. She, "High spectral resolution lidar system with atomic blocking filters for measuring atmospheric parameters," *Appl. Optics* **22**, pp. 1373–1381, 1983.
10. S. T. Shipley, D. H. Tracy, E. W. Eloranta, J. T. Trauger, J. T. Sroga, F. L. Roesler, and J. A. Weinman, "High spectral resolution lidar to measure optical scattering properties of atmospheric aerosols. 1: Theory and instrumentation," *Appl. Optics* **22**, pp. 3716–3724, 1983.
11. J. T. Sroga, E. W. Eloranta, S. T. Shipley, F. L. Roesler, and P. J. Tryon, "High spectral resolution lidar to measure optical scattering properties of atmospheric aerosols. 2: Calibration and data analysis," *Appl. Optics* **23**, pp. 3725–3732, 1983.
12. W. C. Swann and S. L. Gilbert, "Line centers, pressure shift, and pressure broadening of 1530-1560 nm hydrogen cyanide wavelength calibration lines," *J. Opt. Soc. America - B* **22**, pp. 1749–1756, 2005.
13. J. Tuominen, T. Ritari, H. Ludvigsen, and J. C. Petersen, "Gas filled photonic bandgap fibers as wavelength references," *Optics Communications* **255**, pp. 275–277, 2005.